Applications of Imaging Radar Data in Earth Science Investigations

DIANE L. EVANS,
Jet Propulsion Laboratory, California Institute of Technology
Pasadena, CA 91109

Abstract

Synthetic aperture radar (SAR) data provide unique information about Earth's surface and biodiversity, including critical data for natural hazards and resource assessments. The ability to calculate the cross section of a scatterer for any transmit and receive polarization combination provides detailed information about vegetation for assessing changes in land cover, biomass and forest regrowth. Unique SAR interferometric measurements, predominantly large-scale surface change at fine resolution, are used to generate topographic data sets, monitor surface topographic change, and measure glacier ice velocity. The LightSAR Mission, planned for launch in 2002 will be optimized for polarimetric and interferometric data acquisition in order to provide long-term observations of Earth's changing conditions.

1. Introduction

Synthetic aperture radar (SAR) data have become integrated into earth science investigations for many years. Radar sensors provide their own illumination and therefore supply reliable temporal data independent of weather or sun illumination, through all seasons, and at all latitudes. Radar waves penetrate through clouds and, under certain conditions, through vegetation canopies and thin veneers of sand, making it possible to explore regions of the earth's surface that are not accessible using other remote sensing techniques.

SAR data provide unique information about Earth's surface and biodiversity, including critical data for natural hazards and resource assessments. Radar image

brightness is related to radar backscatter at the pixel level, and is a function of land and ocean surface roughness, vegetation canopy structure, and surface dielectric constant. Factors influencing the dielectric constant include temperature of the scattering medium, relative moisture content of vegetation, soil, and snow cover, and the presence of water on vegetation. Thus, it is possible to derive intrinsic physical information about surfaces and volumes that complements measurements made by sensors operating in the visible, short-wave infrared, and thermal infrared portions of the electromagnetic spectrum.

In polarimetric radar systems, the polarization of the scattered wave is measured through a vector measurement process, which permits measurement of the full polarization signature of every resolution element in an image. The ability to calculate the cross section of a scatterer for any assumed transmit and receive polarization combination; horizontally transmitted, horizontally received (HH), vertically transmitted, vertically received (VV), VH, and HV, leads to a more detailed solution for the electrical properties and geometric shape of a surface scatterer. SAR interferometry has also been shown to hold the potential for making major advances in our understanding of Earth processes in several disciplines. Interferometric measurement can be used to generate global topographic maps, to monitor surface topographic change, and to measure glacier ice velocity.

A total of 143 hours (93 terabits) of fully polarimetric L-band (wavelength = 23.5 cm) and C-band (wavelength = 5.8 cm) data, and VV polarized X-band (wavelength = 3.1 cm) data were acquired by the Spaceborne Imaging Radar and X-band Synthetic Aperture Radar (SIR-C/X-SAR) in April and October of 1994. During the October, 1994 flight of SIR-C/X-SAR, over a million square kilometers of repeat-pass SAR interferometry data were obtained. Several orbits were designed to closely duplicate

orbits from the first flight, giving a time separation of approximately six months. Most observations during the last four days of the second flight were devoted to one-day repeat-pass data takes, over several dozen targets around the world.

Single frequency, single polarization interferometry data continue to be acquired by the European Remote-sensing Satellite (ERS), Japanese Earth Resources Satellite (JERS), and Canadian Radarsat Mission (see Table 1 for operating parameters). This paper describes some examples of ecology, solid earth, ice sheets and glaciers, hydrology, and oceanography, studies using data from these sensors as well as from the SIR-C/X-SAR. Much of this material was reported by Evans et al.[1] in 1995 and the authors of that document are gratefully acknowledged.

	-1/2 ERS	JERS-1	SIR-C X-SAR	RADARSAT	LIGHTSAR
Band	C	L	C&L X	C	L
Polarization	VV	HH	Quad	HH	Quad
Resolution (m)	25	18	25	10-100	25-100
Swath Width (km)	100	76	15-100	50-170	50-250
Incidence angles (deg.)	23°	38°	17°-60°	17°-43°	20°-52°
Orbit Repeat time (days)	1, 35	44	1	24	8 or 10
Target Visibility (days)	35	44	1	3	1
Launch Date	7/91 4/95	2/92	4/94 10/94	11/95	2002

Table 1-Recent, Planned and Proposed SAR Missions.

2. Ecology

Kasischke et al.[2] provide a general overview of use of imaging radars for ecological applications. The primary applications of SAR data for ecology are land-cover classification, biomass estimation, and wetland inundation mapping. All of these take

advantage of SAR sensitivity to structure and dielectric constant. In addition, in regions characterized by cloud-cover (e.g., boreal regions, tropical forest and much of Northern Europe), SAR have been used to extend observations made by Landsat and other electro-optical sensors.

Users of land cover classifications include plant and animal ecologists, modelers including those operating general circulation models (GCMs), land managers, government agencies, and economic forecasters. Research dating from the 1960s shows that Ka- and X-band images can be used to produce vegetation cover maps of both natural and cultivated surfaces.[3] More recently, Dobson et al.[4] focused on land-cover classifications for environmental monitoring and commercial forestry applications and found improved classification accuracies by combining polarimetric L-band data with a single polarization data at X-band or dual polarization data at C-band.

A number of studies have shown the power of multidate imagery for enhanced classification results.[5] SAR has proven to be very reliable for provision of multidate data because it is practically insensitive to local weather conditions. Supervised maximum likelihood approaches using multidate single frequency data sets often yield high classification accuracies for a given scene. The calibration stability of existing satellite SARs makes it possible to incorporate time-dependent ancillary information, such as phenological development and cropping calendars, into classification.

The amount and distribution of biomass over the Earth's land surface is one of the major uncertainties in our ability to understand the global carbon cycle. Biomass measurements from SAR are possible in both agricultural fields and natural

vegetation such as pine forests, mixed deciduous and coniferous forests, and rangeland. Single-frequency, single-polarization SARs are sensitive to above-ground biomass differences in forests up to approximately 100 to 150 metric tons per hectare. Multichannel SAR systems, which include a low frequency channel at L-band or P-band (wavelength = 65 cm) and a higher frequency C-band or X-band channel have been used to estimate biomass levels up to 250 to 300 metric tons per hectare. Kasischke et al.,[6] used a two-stage approach to estimate biomass of southern pine forests using C-, L- nad P-band polarimetric data. In step one, total branch biomass was estimated as a function of several different radar frequencies/polarizations. Total biomass was then estimated from branch biomass based upon allometric equations, and resulted in a relative error on the order of 20% for biomass levels up to 400 t ha^{-1}. This biomass range includes all forests except mature old-growth forests in temperate regions and some tropical rain forests.

The ability to penetrate the extensive cloud cover of northern and equatorial latitudes and to detect standing water beneath vegetation canopies makes SAR data particularly valuable for wetland inundation mapping. For example, in northern Alaska, cloud cover and infrequent repeat cycles have limited the acquisition of optical satellite data (Landsat and SPOT) to a total of two scenes for the last 20 years. By comparison, ~50 scenes of ERS-1 SAR data have been acquired for Barrow over a two-year period, and RADARSAT provides daily access.

Inundation is a key indicator of the anaerobic conditions necessary for methane production. Backscatter from ERS-1 SAR acquired over Barrow, Alaska was found to be strongly related to the position of the local water table and thus to methane exchange rates.[7] Backscatter from non-inundated sites was low, that from herbaceous

inundated sites was high, and that from sites with the water table at the surface was intermediate, mirroring methane exchange rates for the region.

In the tropics, delineation of both flooding status and vegetation, with accuracies greater than 90% for all categories, has been demonstrated using multi-frequency, polarimetric SAR data sets for wetlands in the central Amazon.[8] This result is significant in terms of global change, since methane generation rates from floating meadows floodplains of the central Amazon are much higher than those from flooded forest.

SAR data have also been used for malaria risk assessment efforts in Belize and adjacent regions by providing spatial and temporal information on the distribution and flooding status of anopheline breeding sites. Pope et al.[9] used multifrequency, polarimetric airborne SAR data collected over the wetlands in Belize to map *Eleocharis* sp. dominated marshes, which have been shown to be important breeding habitats of the malaria vector *Anopheles albimanus.* Pope et al., (1992) also used airborne X-, C- and L-band SAR data to examine flooding in sedge and grass-covered mosquito larval habitats in Kenya.

3. Solid Earth Sciences and Topography

Geologists were the first to exploit SAR data; early applications included landform mapping and structural interpretation for mineral and oil exploration in perennially cloud-covered regions. The value of SAR for photointerpretation stems from the ability to optimize viewing geometries for different terrain types in a similar way to low sun-angle aerial photography, and the ability to measure surface roughness at scales of the radar wavelength.

The imaging capabilities of SAR are further enhanced by the ability of radar to image beneath thin, dry veneers of sand, exposing subsurface features with potential climatic and tectonic significance.[10] The ability of SAR to penetrate thin sheets of sand cover was highlighted during the SIR-C/X-SAR mission, where subsurface geology of vast areas of the Sahara Desert were revealed for the first time as shown in Figure 1.

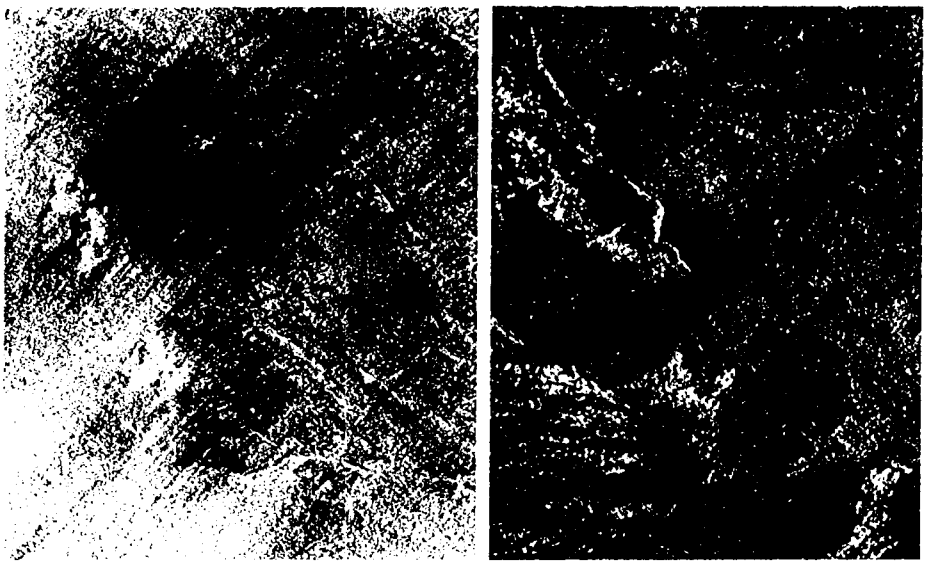

Figure 1-Images of Safsaf oasis in south-central Egypt.

Comparisons of Landsat and SIR-C/X-SAR resulted in the mapping of ancient drainage systems, areas of potential mineralization, and an ancient continental collision zone which provides new insights into the course of the Nile.[11] While these investigations focused on visual comparisons, SAR data have also been used in conjunction with optical and infrared sensor systems in supervised and unsupervised classifications and process response models.

SAR data have also been important for studying volcanoes that are either cloud-covered or obscured by volcanic ash during an eruption. The SIR-C/X-SAR mission afforded opportunities to observe a significant volcanic eruption of Kliuchevskoi volcano on the Kamchatka peninsula[12] (Figure 2).

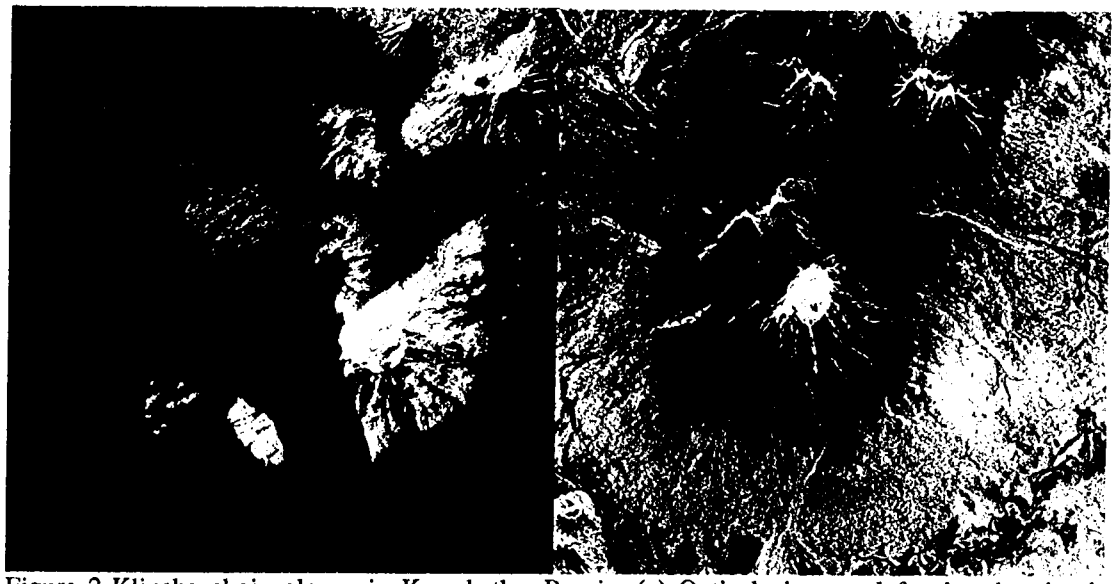

Figure 2-Kliuchevshoi volcano in Kamchatka, Russia: (a) Optical photo at left taken by shuttle astronauts; (b) Radar image at right acquired by SIR-C/X-SAR.

In addition, SIR-C/X-SAR imaged dozens of volcanoes worldwide, including 13 of the 15 Decade Volcanoes designated by the United Nations as the most threatening to humans. These data are being analyzed in conjunction with other remote sensing data sets where they exist. However, in some cases, such some of the Andean Volcanoes, these represent the only available remote sensing data sets because of the perennially cloud cover in the region.

The SIR-C/X-SAR mission afforded opportunities to observe flooding in the state of Illinois and in Germany, and more recently, near real-time observations of floods have been made available over the Internet. Post-flood images are used for quantitative damage assessment, particularly during the immediate post-flood period when the area is still be cloud covered from continuing storms. For the same reason, SAR images may also be useful for rapid damage assessment after major hurricanes, when cloud cover and damaged infrastructure (telephones, roads, bridges) make conventional surveys difficult.

Topographic mapping and topographic change studies using interferometry are thought by many to be among the most compelling uses of SAR for solid-earth studies. Topographic maps derived from cross-track SAR interferometry have been used for a variety of geologic process studies, including determining the history of alluvial fan formation and calculating slope, height, and thickness information for lava flows. Combining several interferometric pairs obtained at a different time allows the measurement of small-scale shifts in the Earth's surface over time.[13, 14] This differential interferometry technique has been used for mapping the effects of earthquakes, monitoring volcanic expansion, mapping advancing lava flows, monitoring landslides and detecting land subsidence due to fluid withdrawal from aquifers or hydrocarbon reservoirs.

Because of the importance of digital topographic data, a global topographic data base will be generated using a reflight of the SIR-C/X-SAR system in September, 1999 using twin antennas separated by a 60 m boom for single-pass interferometry. This Shuttle Radar Topography Mission (SRTM) will provide a digital topographic map of the world equator-ward of 60-degrees latitude, which could then serve as the reference data for future higher resolution topographic and topographic change studies. In a single 11 day Shuttle flight a digital topographic map of 80% of Earth's land surface will be produced with data points spaced every 30 meters and 8 meter relative vertical accuracy. Data sufficient to produce a rectified, terrain-corrected C-band (5.6 cm wavelength) mosaic of 80% of the Earth land surface at 30 meter resolution will also be acquired.

4. Ice Sheets, Glaciers, and Sea Ice

Over 75% of the world's fresh water is presently locked up in ice sheets and glaciers. The expansion and reduction of ice sheets and glaciers from glacial periods to

interglacial periods has been one of the most dramatic climatic signals in Earth history. Even on short time scales of a few years, changes in ice volume have modulated and continue to modulate, sea level. This has never been more important than it is today, given the increase in economic development of coastal areas. While it is certain that small glaciers are experiencing broad retreat and contributing to sea level rise by increased melting, the contributions of the two largest ice sheets in Greenland and Antarctica remain largely unknown.

SAR, with its ability to collect ice-sheet data through cloud and throughout the extended polar night has already demonstrated unique capabilities that make it an indispensable new tool for the glaciologist. Several studies have demonstrated SAR capabilities for monitoring ice-sheet motion, ice topography, glacial surges, and flow dynamics of the Greenland ice sheet.[15] In addition, the Radarsat Antarctic Mapping Mission made it possible to view the vast majority of Antarctica where over 90% of the earth's ice reservoir exists.

Fluxes of heat, momentum, mass, and salt that result from air-sea-ice interactions in the polar oceans also play key roles in global climate. The dynamics and thickness of the sea ice cover are the key elements of these fluxes. Ice motion controls the distribution of thin ice and therefore surface exchange processes dependent on ice thickness, including heat flux to the atmosphere, ice production, and the associated salinity production in the polar oceans. As ice thickens by growth and deformation, the turbulent heat exchange between the ice-covered ocean and the atmosphere is reduced. Detailed time-series measurements of ice motion and thickness from satellite sensors are essential in providing estimates of these fluxes.

During the last several years, maps of the vector motions of Arctic sea ice have been automatically generated from SAR data by the Alaska SAR Facility (ASF).[16] SAR images taken three or more days apart and then derives their absolute motion relative to a fixed geographical grid. For areas in which there are significant oceanic fluxes, a direct measurement of ice thickness over time is the optimal approach for deriving heat and salinity transport. There are good indications that ice thicknesses of less than 100 cm can be estimated using the like-channels (HH and VV) of a polarimetric L-Band SAR.[17] Copolar phases ranging from –50° to +30° have been observed in ice of differing apparent thickness; such values span both lower-than-expected values for thick ice and higher-than-expected values for open water. A model has been developed that explains these variations, and it has considerable potential for estimating sea ice thickness using magnitudes and phases of SAR data. An example from SIC-C/X-SAR is shown as Figure 3.

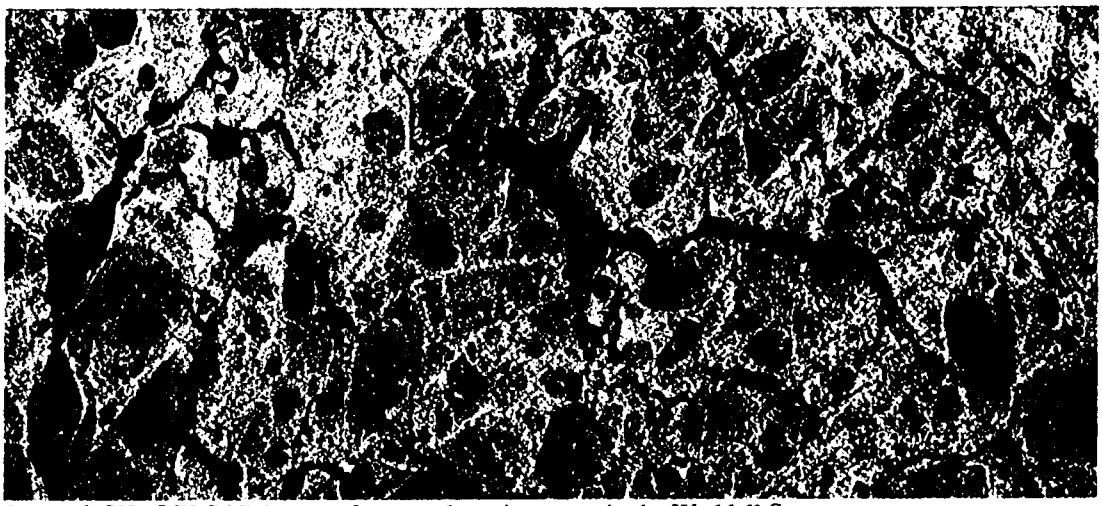

Figure 3-SIR-C/X-SAR image of seasonal sea-ice cover in the Weddell Sea.

5. Hydrology

Soil moisture is a critical parameter for both the agricultural community and ecosystem modelers. Over the past decade or so, much research into the use of remote sensing to measure soil moisture has taken place. Truck-mounted, aircraft, and

spaceborne SAR measurements from the 1960s to the present have confirmed the correlation of radar backscatter with surface soil moisture. Measurements show that the estimated soil moisture for L-band frequencies correlate best with soil moistures in the top 5 cm of the soil. However, the nature of the interaction between a radar signal and the terrain is strongly affected by surface roughness, slope, and vegetation cover.

Several algorithms have been developed, ranging from empirical models to ones based on complex electromagnetic scattering theories to separate the effects of surface roughness and soil moisture. All these algorithms give similar results, with proven accuracies, compared to *in situ* measurements, of on the order of 4% volumetric soil moisture at spatial scales of a few tens of meters.[18]

Measurements of snow properties, snow cover and snow-water equivalence are also being investigated with SAR data. Recent studies (using SIR-C/X-SAR and ERS-1 data) have shown a significant improvement in understanding and modeling the backscattering and polarization properties as a function of snow-pack parameters. An accurate algorithm to retrieve snow wetness, which indicates where and at what rate snow is melting, has been developed and tested using C-band polarimetric data.[19] Thus, accurate information about the spatial and temporal distributions and melting status of snow cover can be provided for hydrological and climatic investigations and operations. Maps of snow-covered area derived from SIR-C/X-SAR also compare reasonably well (85-90% accuracy) with those derived from visible imagery, which require clear weather and daylight.

6. Oceanography

The open ocean process that has been best studied by SAR are long surface waves, their spatial spectra, and their refraction patterns. Long-term observations of ocean wave spectra could allow studies of exchange of momentum between atmosphere and ocean, especially during storm conditions. In addition, wave refraction by large-scale current systems such as the Gulf Stream is readily observed in high-resolution images, and provides estimates of the current speed under some conditions. [20]

Although coastal oceans and estuaries comprise about 10% of the Earth's surface, they produce about 25% of global biomass production. In the coming decades, the effects of global change and human activities will be especially pronounced in the coastal zone In coastal oceanography, single-frequency, single-polarization SARs have demonstrated their ability to record internal waves, surface waves, bathymetric features, and the location of ocean fronts.

Wind-driven offshore transport and turbulent mixing have important effects on the larval survival and subsequent recruitment of many fish species. Space-based SAR can locate current boundaries, fronts, convergence zones, eddies, and ice fields, all of which influence commercially-important fish populations. Detection of natural and man-made slicks on the sea is also crucial to the protection of the environment and the enforcement of regulations. In order to demonstrate the signatures of various types of oils and other surfactants such as oleic acids, a controlled release of oils and surfactants in the North Sea was made recently by German scientists and imaged by SIR-C/X; the slicks are readily detectable and appear as regions of variously reduced backscatter another example from SIR-C/X-SAR is shown as Figure 4.

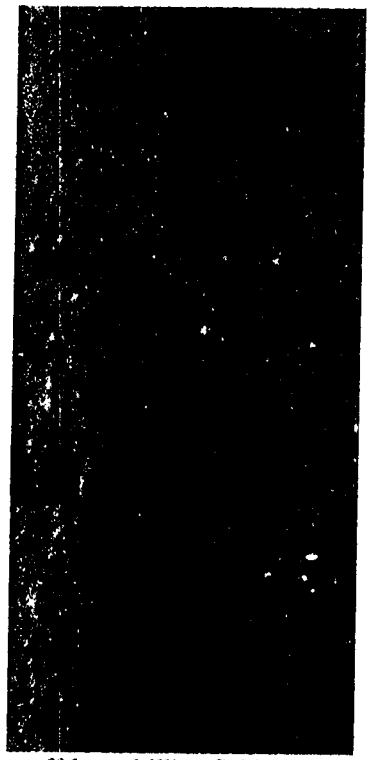

Figure 4- SIR-C image of an offshore drilling field about 150km west of Bombay, India, in the Arabian Sea.

7. Conclusions

The paper demonstrates that the suite of spaceborne SAR systems currently flying by the international community provide an important data for addressing key science issues and applications. These measurements will be augmented by L-band interferometric and polarimetric measurements made by the LightSAR, a mission planned for launch in 2002 which would make use of advances in materials science and hybrid structures, and microelectronics to reduce mission costs.

Acknowledgments

This publication was prepared by the Jet Propulsion Laboratory, California Institute of Technology, under a contract with the National Aeronautics and Space Administration. It contains material from contributors in United States government agencies, agencies of other governments, universities, and private industry.

Contributors to the original document from which much of this material was condensed are:

John Apel, Applied Physics Laboratory

Ray Arvidson, Washington University

Robert Bindschadler, Goddard Space Flight Center

Frank Carsey, Jet Propulsion Laboratory

Jeff Dozier, University of California, Santa Barbara

Ken Jezek, Ohio State University

Eric Kasischke, ERIM/Duke University

John Melack, University of California, Santa Barbara

Bernard Minster, University of California, San Diego

Pete Mouginis-Mark, University of Hawaii

Jakob van Zyl, Jet Propulsion Laboratory

References

1. EVANS, D., KASISCHKE, E., MELACK, J., DOZIER, J., VAN ZYL, J., APEL, J., CARSEY, F., BINDSCHADLER, R., JEZEK, K., ARVIDSON, R., MINSTER, B., MOUGINIS-MARK, P., LI, F. SKOLNICK, M., (1995) Spaceborne Synthetic Aperture Radar: Current Status and Future Directions, NASA Technical Memorandum 4679, 171 pgs.

2. KASISCHKE, E. MELACK, J., and DOBSON, C. (1997), The use of imaging radars for ecological applications-a review, *Remote Sensing of Environment,* vol. 59, no. 2, p141-156.

3. ULABY, F.T., MOORE, R. and FUNG, A. 1986, in Microwave Remote Sensing: Active and Passive. Vol. 3. Artech House, Dedham, Mass.

4. DOBSON, M., PIERCE, L.E. and ULABY, F.T. 1997. "The Role of Frequency and Polarization in Terrain Classification Using SAR Data." Pp. 1621-1623 in Remote Sensing - A Scientific Vision for Sustainable Development. Proceedings, International Geoscience and Remote Sensing Symposium. Vol. 4. IEEE, New York.

5. RANSON, J. K. and SUN, G. (1994). Northern forest classification using temporal multifrequency and multipolarimetric SAR images. Rem. Sens. Environ., vol. 47, pp. 142-153.

6. KASISCHKE, E. S., CHRISTENSEN, JR., N. L. and BOURGEAU-CHAVEZ, L. L. (1995). Correlating radar backscatter with components of biomass in loblolly pine forests. IEEE Trans. Geosci. Rem. Sens., vol. 33 643-659.

7. MORRISSEY, L. A., LIVINGSTON, G. P. and DURDEN, S. L. (1994). Use of SAR in regional methane exchange studies. Int. J. Rem. Sens., vol. 15, pp. 1337-1342.

8. HESS, L. L., MELACK, J. M., FILOSO, S., and WANG, Y. (1995). Delineation of inundated area and vegetation along the Amazon floodplain with the SIR-C synthetic aperture radar. IEEE Trans. Geosci. Rem. Sens. vol. 33 no. 4 p.896-904.

9. POPE, K. O., REY-BENAYAS, J. M., and PARIS, J. F. (1994). Radar remote sensing of forest and wetland ecosystems in the Central American tropics. Rem. Sens. Environ., vol. 48, pp. 205-219.

10. MCCAULEY, J. F., SCHABER, G. G., BREED, C. S., GROLIER, M. J., HAYNES, C. V., ISSAWI, B., ELACHI, C., and BLOM, R. (1982). Subsurface valleys and geoarcheology of the eastern Sahara revealed by Shuttle radar. Science, vol. 218, pp. 1004-1020.

11. ABDELSALAM, M. G. and STERN, R.J., 1996. Mapping Precambrian structure in the Sahara desert with SIR-C/X-SAR radar: Neoproterozoic Keraf Suture, NE Sudan, *Journal of Geophysical Research*, 101, E10, 23,063-23,076.

12. EVANS, D.L., PLAUT, J.J. and STOFAN, E.R. (1997) Overview of the Spaceborne Imaging Radar-C / X-band Synthetic Aperture Radar (SIR-C/X-SAR) Missions, Remote Sensing of Environment, vol. 59, no. 2, p. 135-140.

13. MASSONNET, D., BRIOLE, P. and ARNAUD, A. 1995. "Deflation of Mount Etna Monitored by Spaceborne Radar Interferometry." Nature 375:567-570.

14. ZEBKER, H. A., ROSEN, P. A. GOLDSTEIN, R. M. GABRIEL, A. WERNER, C. L. "On the derivation of co-seismic displacement fields using differential radar interferometry: The Landers earthquake," *J. Geophys. Res.*, vol. 99, p. 19617, 1994.

15. JOUGHIN, I., WINEBRENNER, D. FAHNESTOCK, M.A. KWOK, R. and KRABILL, W. 1996b. "Measurement of Ice-Sheet Topography Using Satellite Radar Interferometry." J. Glaciology 42(140):10-22.

16. KWOK, R., ROTHROCK, D.A., STERN, H., and CUNNINGHAM, G. (1995). Determination of ice age from Lagrangian observations of ice motion. IEEE Trans. Geoscience and Remote Sensing, vol. 33, No. 2, pp. 392-400.

17. DRINKWATER, M., KWOK, R., RIGNOT, E., ISRAELSSON, H., ONSTOTT, R., and WINEBRENNER, D. (1992). Potential applications of polarimetry to the classification of sea ice, in Microwave Remote Sensing of Sea Ice (F. Carsey, ed.). Geophysical Monograph 68, AGU, Washington, D.C., pp. 419-430.

18. DUBOIS, P.C., VAN ZYL, J. J. and ENGMAN, E. T. (1995). Measuring soil moisture with imaging radars, IEEE Trans. Geosci. Rem. Sens. vol. 33 no. 4 p. 915-926

19. SHI, J. and DOZIER, J. (1995). Inferring snow wetness using SIR-C's C-band polarimetric synthetic aperture radar. IEEE Trans. on Geosci. and Rem. Sens. vol. 33 no. 4 p. 905-914

20. LIU, A., PENG, C., and SCHUMACHER, J. 1994. "Wave-current Interaction Study in the Gulf of Alaska for the Detection of Eddies by SAR." J. Geophys. Res. 99:10075-10085.

Captions to Figures.

Figure 1. These images are of Safsaf oasis in south-central Egypt where field studies indicate that L-band radar can penetrate as much as 2 m. Each image is 30.8 kilometers by 25.6 kilometers and is centered at 22.7 degrees north latitude, 29.3 degrees east longitude. North is toward the upper right.

Left: Landsat image, the colors are assigned as follows: red is Band 7 (mid-infrared); green is Band 4 (near infrared); and blue is Band 1 (visible blue light).

Right: SIR-C/X-SAR image: red is L- band, horizontally transmitted and received; green is C-band, horizontally transmitted and received; and blue is X-band, vertically transmitted and received.

Figure 2. This comparison shows optical and radar imaging of Kliuchevshoi volcano in Kamchatka, Russia, which began to erupt on September 30, 1994. The optical photo at left was taken by shuttle astronauts during the early hours of the eruption on September 30. The ash plume, which reached heights of more than 18 kilometers, is emerging from a vent on the north flank of Kliuchevskoi, partially hidden by the plume and its shadow in this view. The photograph is oriented with north toward the bottom, for comparison with the radar image at right acquired a few days later. Near the center of the photo, a small whitish steam plume may be seen emanating from the growing lava dome of a companion volcano, Bezymianny.

In the radar image at right, Kliuchevskoi is the blue triangular peak in the center of the image, towards the left edge of the bright red area that delineates bare snow cover. The image was acquired by SIR-C/X-SAR on October 5, 1994. The image shows an area approximately 75 kilometers by 100 kilometers that is centered at 56.07 degrees north latitude and 160.84 degrees east longitude. North is toward the bottom of the image. The radar illumination is from the top of the image. The colors in this image were obtained using the following radar channels: red represents the L- band (horizontally transmitted and received); green represents the L-band (horizontally transmitted and vertically received); blue represents the C-band (horizontally transmitted and vertically received).

Figure 3. SIR-C/X-SAR image of seasonal sea-ice cover in the Weddell Sea, acquired on October 3, 1994 Red is C-band, HH-polarization, green is L-band, HV-polarization, and blue is L-band, HH-polarization). The image is oriented almost east-west with a center location of 58.2 degrees South and 21.6 degrees East. Image dimensions are 45 kilometers by 18 kilometers. Most of the ice cover is composed of rounded, undeformed blue-gray floes, about 0.7 meters thick, which are surrounded by a jumble of red-tinged deformed ice pieces which are up to 2 meters thick. The bright red lines are an intermediate stage of new ice growth perhaps 5 to 10 centimeters. The more extensive dark zones are covered by a slightly thicker layer of smooth, level ice up to 70 centimeters thick.

Figure 4. This is a SIR-C image of an offshore drilling field about 150 km west of Bombay, India, in the Arabian Sea. The dark streaks are extensive oil slicks surrounding many of the drilling platforms, which appear as bright white spots. Radar images are useful for detecting and measuring the extent of oil see pages on the ocean surface, from both natural and industrial sources. The long, thin streaks extending from

many of the platforms are spreading across the sea surface, pushed by local winds. The larger dark patches are dispersed slicks that were likely discharged earlier than the longer streaks, when the winds were probably from a different direction. The dispersed oil will eventually spread out over the more dense water and become a layer which is a single molecule thick. Many forms of oil, both from biological and from petroleum sources, smooth out the ocean surface, causing the area to appear dark in radar images. There are also two forms of ocean waves shown in this image. The dominant group of large waves (upper center) are called internal waves. These waves are formed below the ocean surface at the boundary between layers of warm and cold water and they appear in the radar image because of the way they change the ocean surface. Ocean swells, which are waves generated by winds, are shown throughout the image but are most distinct in the blue area adjacent to the internal waves. Red is L-band vertically transmitted, vertically received; green is the average of L-band vertically transmitted, vertically received and C-band vertically transmitted, vertically received; blue is C-band vertically transmitted, vertically received. The image is located at 19.25 degrees north latitude and 71.34 degrees east longitude and covers an area 20 km by 45 km.

Figure1

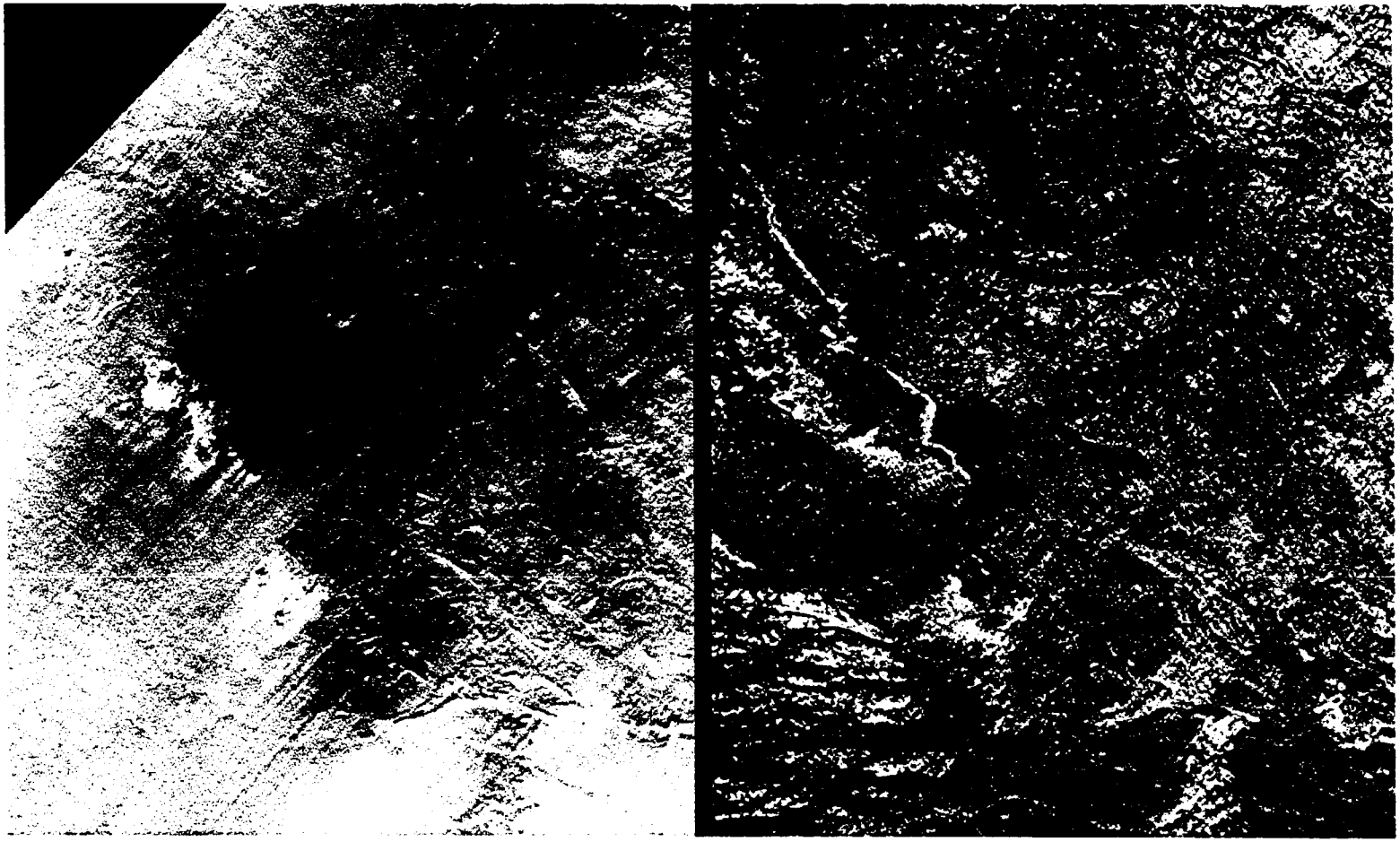

Figure 2

Figure 2

Figure 3

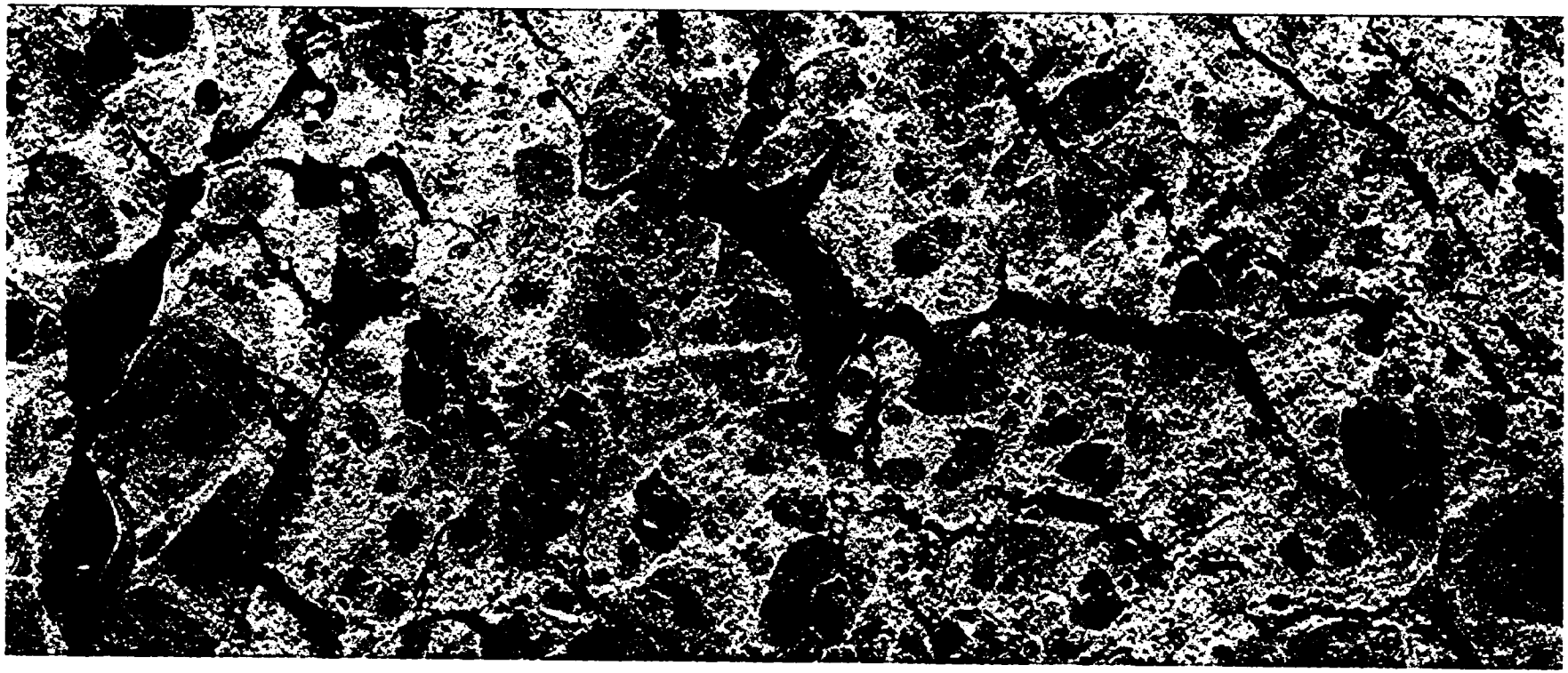

orientation

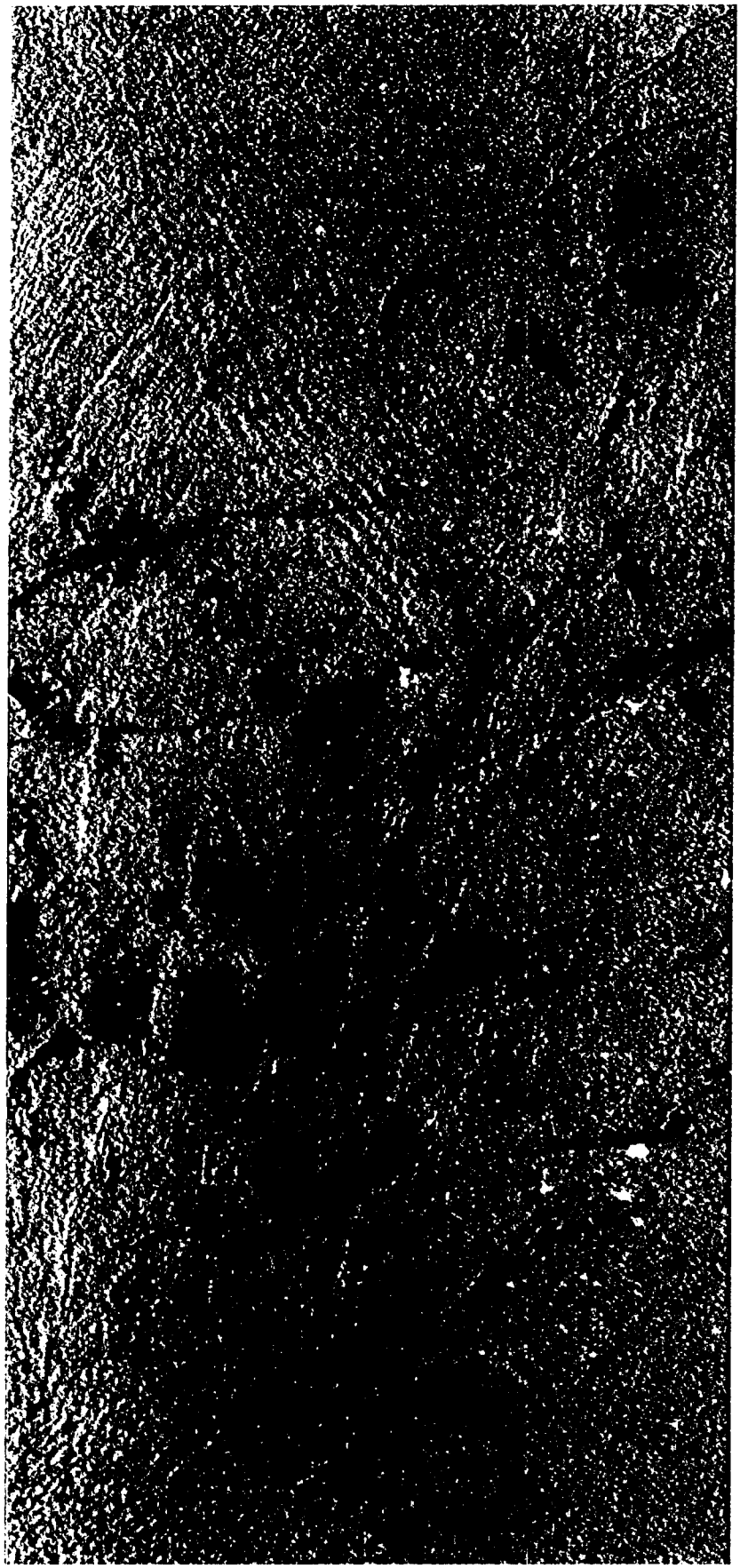

Figure 4